Chapter 4

Study of an interfacial semi-infinite crack in a composite structure

4.1 Introduction

4.1.1 Background

Interfacial cracks are a phenomenon that typically manifests along the boundary between two distinct materials or at the interfaces within a layered composite material. These cracks can materialize during fabrication, even before any load is applied, forming microcracks.. In the context of orthotropic materials, characterized by varying mechanical properties in different directions, interfacial cracks can develop between layers with disparate orientations. This occurrence can profoundly

impact the mechanical performance and the overall reliability of the structures composed of these materials. The behaviour of interfacial cracks in orthotropic materials is a critical factor in comprehending the structural integrity of a component and the mechanisms leading to its failure. Given the anisotropic nature of these materials, the complexity associated with interfacial cracks is significantly higher than their isotropic counterparts. This complexity necessitates a thorough investigation to ensure the structural soundness of components made from orthotropic materials.

4.1.2 Literature survey and research gaps

Some analytic studies of interface cracks in isotropic media can be found in [74, 75, 76]. The oscillatory singularities obtained while dealing with interfacial cracks were determined in these research articles. Furthermore, the investigations of interfacial cracks in anisotropic materials can be found in early works [107, 78, 79, 80, 81]. Willis has worked on a finite crack in dissimilar anisotropic half-planes in his work [83]. He studied the infinite stresses near the tip of the contact region. With his work, Ting [80] concluded that displacement oscillation is dependent on the material properties only and independent of the individual orientation of the materials. Several methods, like integral transforms and the function approach, have been explored to solve the interface crack problem and its singularities. The finite crack present in an infinite orthotropic strip under normal loading is investigated in the study of Shindo et al. [108].

In antiplane shear, a single displacement field perpendicular to the plane of interest complementary to the two in-plane displacements is generally considered in most solid mechanics problems. antiplane crack problems have often been solved for homogenous, isotropic solids [94, 109, 110]. The near-crack tip stress field analysis has been discussed in detail. Ru [109] has used the complex variable method and

the theory of analytic functions for his study. The antiplane loading problem with a crack at the interface of the orthotropic strips was tackled in [111]. A brief and well-encapsulated review of antiplane models has been done in [104] for linear and non-linear problems. Most recently, analytic studies of the mode III interface crack can be found in [112, 113]. Semi-infinite planes containing semi-infinite cracks have been dealt with in [114, 115]. A problem of a semi-infinite plate with an oblique edge crack in an orthotropic medium has been solved in [116], where the author calculated the SIF for mode I and mode II. Wiener-Hopf method [117] is an extension of the Fourier transform method in which convolution kernels are assumed on a semi-infinite line and then factorised into known functions. This method uses the concepts of complex-valued analytic functions and has been proven effective in solving problems with semi-infinite boundaries [118, 119]. Since then, due to the applicability of this method in real-world applications, many research works have been devoted to the method, and many attempts have been made to extend the method for a system of integral equations. This chapter focuses on the W-H method applied to an antiplane shear problem for a single integral equation. The original problem is converted into a W-H equation.

Although many studies have been done in this area, The antiplane problems addressing moving cracks in dissimilar orthotropic mediums are limited. Yoffee in [120] introduced the moving crack problem with a straight crack moving with a constant speed in an elastic medium. Knauss [114] solved the problem of stresses in an infinitely long isotropic strip of finite width containing a straight semi-infinite crack for the case of displaced clamped boundaries normal to the crack. He applied the Wiener–Hopf technique to find the SIF and stresses. Rice [121] corrected this work in his problem. Using the Wiener-Hopf method, Nilsson [122] gave the analytic expression for a semi-infinite crack in an isotropic strip for both clamped

and free boundary conditions. Later, many authors [123, 124, 125] used the same technique in their respective works. Recently, [126, 127] have addressed the problems of semi-infinite cracks in dissimilar strips. Basak calculated the SIF and crack opening displacements for a crack inside an orthotropic strip. Itou [128] considered the problem of moving Griffith crack between two distinct half-planes. He used the Schmidt method to solve the unknown coefficient series for his problem.

Based on coupled stress theory, Itou has worked on many problems [129] and studied interface cracks to exhibit square-root singularity near the crack end and length-dependent strain energy release rate. Wang [130] also applied this couple stress theory together with the electric field gradient to analyse a mode-III crack problem in piezoelectric materials, and singularity of both $r^{-1/2}$ and $r^{-3/2}$ is obtained. In interface cracks, oscillatory singularities occur, which is different from the squared-root singularity seen in the homogenous isotopic medium.

In this problem, an interfacial semi-infinite crack in a composite orthotropic media under an antiplane is studied with the Wiener-Hopf method. A drive has been given to calculate the SIF at the tip of the cracks having the singularity with order $r^{-1/2+\iota\epsilon}$, $\epsilon > 0$. To date, no research has found the SIF considering the said singularity. The authors of this chapter have taken a challenge to it and successfully found the expression of SIF, which is the first of its kind. Hope this will help the researchers working in the area of infinite/semi-infinite cracks in composite media. The crack energy release rate is also found. The propagation of the crack along the interface is shown graphically through calculations of the SMF. Another important point of this study is finding the length of the wrinkle near the surface of the tip of the interfacial semi-finite crack, which is also the first of its kind. The authors have considered the case of a single contact zone near the crack tip subjected to shear loading. The significance of the length of the contact zone at the interface of

two dissimilar materials has been considered, and the calculations have been carried out for the same. The inclusion of the semi-infinite contact zone is necessary to exclude the possibility of overlapping cracks. The innovative aspect of the chapter is centered around the computation of the SIF that exhibits an oscillating singularity, the amplification of the crack employing the Stress Magnification Factor (SMF), and the determination of the contact zone length proximate to the crack tip at the interface of the crack. The chapter meticulously calculates and graphically represents the SIF at the crack tip, the SMF, and the energy released due to the crack. This comprehensive approach provides a novel perspective in the study of material stress and crack propagation.

4.1.3 Chapter organisation

The chapter addresses the problem of a moving semi-infinite crack present at the interface of orthotopic strips. For the problem, The antiplane governing equations have been formulated in Section 4.2 where material densities, SH-wave velocities and appropriate transformation have been applied. Section 4.3 discussed the different boundary conditions that are required in the positive and negative half-planes. In the section, expressions of displacements and shear stresses have also been established. The solution procedure to the said problem has been discussed in detail in Section 4.4 where the sub-section 4.4.1 is devoted to the Wiener-Hopf method and the decomposition of the kernel. As a result, the expression for unknown functions has been obtained by utilising the concepts of analyticity and integral formulas. Section 4.5 contains the obtained expressions of mode-III SIF, crack energy. A particular case of the present problem has been discussed in Sub-section 4.5.1, which has been used to calculate the stress magnification factor. A detailed Numerical result and discussion for the obtained plots for different parameters under different

particular cases have been given in Section 4.6. The last section of the chapter 4.7 contains the concluding remarks about the whole study presented in the current chapter.

4.2 Governing equations

Consider a moving semi-infinite crack situated at the interface of an infinite orthotropic strip 1 $(-\infty < X < \infty, 0 \leq Y \leq h)$ bonded to a distinct infinite orthotropic strip 2 $(-\infty < X < \infty, -h \leq Y \leq 0)$. Strip 1 and strip 2 are bonded with the infinite orthotropic strip 3 $(-\infty < X < \infty, h \leq Y \leq h_1)$ and strip 4 $(-\infty < X < \infty, -h_1 \leq Y \leq -h)$, respectively. Let the crack propagate towards positive X-direction with a constant velocity V. The crack is positioned at $-\infty < X < 0, Y = 0$ as shown in Figure 4.1. At a time instant t, the crack is positioned at $Y = 0, -\infty < X < Vt$. The crack surface is considered under antiplane shear loading. In what follows and in the sequel, the quantities with subscripts $j = 1, 2, 3, 4$ refer to those for strip 1, strip 2, strip 3 and strip 4, respectively. The

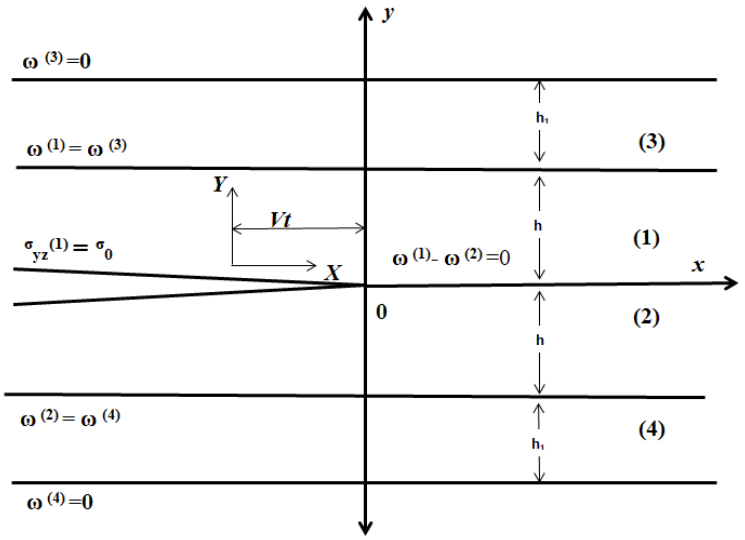

FIGURE 4.1: Geometry of the problem.

governing equations of motion In antiplane are given by

$$C_{55}^{(j)}\ \frac{\partial^2 W^{(j)}}{\partial X^2} + C_{44}^{(j)}\ \frac{\partial^2 W^{(j)}}{\partial Y^2} = \rho^{(j)}\ \frac{\partial^2 W^{(j)}}{\partial t^2}, \tag{4.1}$$

where $\rho^{(j)}$ represent the material densities of the respective strips. Rewriting equation (4.1) as

$$\frac{\partial^2 W^{(j)}}{\partial X^2} + (\alpha^{(j)})^2\ \frac{\partial^2 W^{(j)}}{\partial Y^2} = \frac{1}{(C_s^{(j)})^2}\frac{\partial^2 W^{(j)}}{\partial t^2}, \tag{4.2}$$

where $\alpha^{(j)}=\sqrt{C_{44}^{(j)}/C_{55}^{(j)}}$. Here, $C_s^{(j)} = \sqrt{C_{55}^{(j)}/\rho^{(j)}}$ are the SH-wave velocities. The displacement component $W^{(j)} = W^{(j)}(X, Y, t)$ for the problem is found in the Z-direction only, i.e., out-of-plane direction. Applying the Galilean transformation by substituting $x = X - Vt$, $y = Y$ in equation (4.2), the problem is converted from time-dependent to free from time t as given below

$$H^{(j)^2}\frac{\partial^2 \omega^{(j)}}{\partial x^2} + \frac{\partial^2 \omega^{(j)}}{\partial y^2} = 0, \tag{4.3}$$

where $H^{(j)}=\sqrt{\frac{1}{\alpha^{(j)2}}(1-\frac{V^2}{C_s^{(j)2}})}$ and $\omega^{(j)} = \omega^{(j)}(x, y)$. The crack defined by $-\infty < x < 0$, $y = 0$ is assumed to be opened by internal traction σ_0 on the crack face.

4.3 Boundary conditions and problem formulation

Thus, the continuity and boundary conditions on $y = 0$ are

$$\tau_{yz}^{(1)}(x, 0) = \sigma_0, \quad -\infty < x < 0, \tag{4.4a}$$

$$\tau_{yz}^{(1)}(x,0) = \tau_{yz}^{(2)}(x,0), \qquad -\infty < x < \infty, \tag{4.4b}$$

$$\omega^{(1)}(x,0) = \omega^{(2)}(x,0), \qquad 0 < x < \infty. \tag{4.4c}$$

The boundary conditions on $y = \pm h$ are

$$\tau_{yz}^{(1)}(x,h) = \tau_{yz}^{(3)}(x,h), \qquad -\infty < x < \infty, \tag{4.4d}$$

$$\omega^{(1)}(x,h) = \omega^{(3)}(x,h), \qquad -\infty < x < \infty, \tag{4.4e}$$

$$\tau_{yz}^{(2)}(x,-h) = \tau_{yz}^{(4)}(x,-h), \qquad -\infty < x < \infty, \tag{4.4f}$$

$$\omega^{(2)}(x,-h) = \omega^{(4)}(x,-h), \qquad -\infty < x < \infty. \tag{4.4g}$$

The boundary conditions on $y = \pm(h + h_1)$ are

$$\omega^{(3)}(x,h+h_1) = 0, \qquad -\infty < x < \infty, \tag{4.4h}$$

$$\omega^{(4)}(x,-h-h_1) = 0, \qquad -\infty < x < \infty, \tag{4.4i}$$

where $\omega^{(j)}$ and $\tau_{yz}^{(j)}$ for $j = 1, 2, 3, 4$ are the respective displacements and stresses of the strips. Now, using the Fourier transform on equation (4.3) as

$$\begin{aligned}\bar{\omega}^{(j)}(s, y) &= F[\omega^{(j)}(x, y) : x \to s], \\ &= \frac{1}{\sqrt{2\pi}} \int_{-\infty}^{\infty} \omega^{(j)}(x, y) e^{isx} dx, \quad j = 1, 2, 3, 4,\end{aligned} \tag{4.5}$$

where $s = \alpha + \iota\gamma$ is a complex variable. The solutions are assumed in the form of

$$\bar{\omega}^{(1)}(s, y) = A^{(1)}(s)\ e^{-H^{(1)}sy} + B^{(1)}(s)\ e^{H^{(1)}sy}, \tag{4.6a}$$

for strip 1.

$$\bar{\omega}^{(2)}(s, y) = A^{(2)}(s)\ e^{-H^{(2)}sy} + B^{(2)}(s)\ e^{H^{(2)}sy}, \tag{4.6b}$$

for strip 2.

$$\bar{\omega}^{(3)}(s, y) = A^{(3)}(s)\ e^{-sH^{(3)}(h+h_1)}\ [e^{-sH^{(3)}(y-h-h_1)} - e^{sH^{(3)}(y-h-h_1)}], \tag{4.6c}$$

for strip 3.

$$\bar{\omega}^{(4)}(s, y) = A^{(4)}(s)\ e^{sH^{(4)}(h+h_1)}\ [e^{-sH^{(4)}(y-h-h_1)} - e^{sH^{(4)}(y-h-h_1)}], \tag{4.6d}$$

for strip 4. where $A^{(1)}(s)$, $A^{(2)}(s)$, $A^{(3)}(s)$, $A^{(4)}(s)$, $B^{(1)}(s)$, $B^{(2)}(s)$ are unknown coefficients to be determined . Using the relation

$$\tau_{yz}^{(j)} = C_{44}^{(j)} \frac{\partial \omega^{(j)}}{\partial y}, \quad \text{for } j = 1, 2, 3, 4, \tag{4.7}$$

we obtain the corresponding antiplane stress components as

$$\bar{\tau}_{yz}^{(1)}(s, y) = C_{44}^{(1)}\ H^{(1)}s\ (-A^{(1)}(s)\ e^{-H^{(1)}sy} + B^{(1)}(s)\ e^{H^{(1)}sy}), \tag{4.8a}$$

$$\bar{\tau}_{yz}^{(2)}(s,y) = C_{44}^{(2)}\ H^{(2)}s\ (-A^{(2)}(s)\ e^{-H^{(2)}sy} + B^{(2)}(s)\ e^{H^{(2)}sy}), \tag{4.8b}$$

$$\bar{\tau}_{yz}^{(3)}(s,y) = -\ C_{44}^{(3)}\ H^{(3)}s\ e^{-sH^{(3)}(h+h_1)}\ [e^{-sH^{(3)}(y-h-h_1)} + e^{sH^{(3)}(y-h-h_1)}]\ A^{(3)}(s), \tag{4.8c}$$

$$\bar{\tau}_{yz}^{(4)}(s,y) = -\ C_{44}^{(4)}\ H^{(4)}s\ e^{-sH^{(4)}(h+h_1)}\ [e^{-sH^{(4)}(y-h-h_1)} + e^{sH^{(4)}(y-h-h_1)}]\ A^{(4)}(s). \tag{4.8d}$$

To employ the W-H technique, the modified boundary conditions of equation (4.4a) is written as

$$\tau_{yz}^{(1)}(x,0) = \sigma_0\ e^{\epsilon x}, \qquad -\infty < x < 0, \tag{4.9}$$

where $\epsilon \to 0$.

Applying equation (4.5), in the transformed domain, the continuity and boundary conditions in equation (4.4) becomes

$$\bar{\tau}_{yz}^{(1)}(s,0) = \frac{\sigma_0}{\sqrt{2\pi}(\epsilon + \iota s)}, \qquad -\infty < s < 0, \tag{4.10a}$$

$$\bar{\tau}_{yz}^{(1)}(s,0) = \bar{\tau}_{yz}^{(2)}(s,0), \qquad -\infty < s < \infty, \tag{4.10b}$$

$$\bar{\omega}^{(1)}(s,0) = \bar{\omega}^{(2)}(s,0), \qquad 0 < s < \infty, \tag{4.10c}$$

$$\bar{\tau}_{yz}^{(1)}(s,h) = \bar{\tau}_{yz}^{(3)}(s,h), \qquad -\infty < s < \infty, \tag{4.10d}$$

$$\bar{\omega}^{(1)}(s,h) = \bar{\omega}^{(3)}(s,h), \qquad -\infty < s < \infty, \tag{4.10e}$$

$$\bar{\tau}^{(2)}_{yz}(s,-h) = \bar{\tau}^{(4)}_{yz}(s,-h), \qquad -\infty < s < \infty, \tag{4.10f}$$

$$\bar{\omega}^{(2)}(s,-h) = \bar{\omega}^{(4)}(s,-h), \qquad -\infty < s < \infty, \tag{4.10g}$$

$$\bar{\omega}^{(3)}(s,h+h_1) = 0, \qquad -\infty < s < \infty, \tag{4.10h}$$

$$\bar{\omega}^{(4)}(s,-h-h_1) = 0, \qquad -\infty < s < \infty. \tag{4.10i}$$

For the integration in equation (4.10a) to be valid, $\gamma < \epsilon$ should follow. From the interfacial boundary conditions on equations (4.10d) and (4.10e) with the aid of equations (4.6a), (4.6c), (4.8a), (4.8c), give rise to

$$B^{(1)}(s) = \left(\frac{(\eta_1 - 1) - (\eta_1 + 1)\ e^{-2sH^{(3)}h_1}}{(\eta_1 + 1) - (\eta_1 - 1)\ e^{-2sH^{(3)}h_1}} \right) e^{-2sH^{(1)}h} A^{(1)}(s), \tag{4.11}$$

where $\eta_1 = \frac{C^{(1)}_{44}\ H^{(1)}}{C^{(3)}_{44}\ H^{(3)}}$.

The boundary conditions equations (4.10f) and (4.10g) with the aid of equations (4.6b), (4.6d), (4.8b), (4.8d), give

$$A^{(2)}(s) = \left(\frac{(\eta_2 - 1) - (\eta_2 + 1)\ e^{-2sH^{(4)}h_1}}{(\eta_2 + 1) - (\eta_2 - 1)\ e^{-2sH^{(4)}h_1}} \right) e^{-2sH^{(2)}h} B^{(2)}(s), \tag{4.12}$$

where $\eta_2 = \frac{C_{44}^{(2)}\ H^{(2)}}{C_{44}^{(4)}\ H^{(4)}}$.

The continuity condition equation (4.10b) give

$$B^{(2)}(s) = \eta_3 \frac{\left(-1 + \frac{(\eta_1-1)-(\eta_1+1)\ e^{-2sH^{(3)}h_1}}{(\eta_1+1)-(\eta_1-1)\ e^{-2sH^{(3)}h_1}} \right) e^{-2sH^{(1)}h}}{1 - \left(\frac{(\eta_2-1)-(\eta_2+1)\ e^{-2sH^{(4)}h_1}}{(\eta_2+1)-(\eta_2-1)\ e^{-2sH^{(4)}h_1}} \right) e^{-2sH^{(2)}h}} A^{(1)}(s), \tag{4.13}$$

where $\eta_3 = \frac{C_{44}^{(1)}\ H^{(1)}}{C_{44}^{(2)}\ H^{(2)}}$.

4.4 Solution Procedure

To proceed further in the problem, we first consider two unknown functions $f(x)$ and $g(x)$ given by

$$\tau_{yz}^{(1)}(x,0) = f(x), \qquad 0 < x < \infty, \tag{4.14a}$$

$$\omega^{(1)}(x,0) - \omega^{(2)}(x,0) = g(x), \qquad -\infty < x < 0. \tag{4.14b}$$

Taking Fourier integral transform on equations (4.14), we obtain

$$\bar{\omega}^{(1)}(s,0) - \bar{\omega}^{(2)}(s,0) = \bar{g}(s), \qquad -\infty < s < \infty, \tag{4.15}$$

$$\bar{\tau}_{yz}^{(1)}(s,0) = \bar{f}(s) + \frac{\sigma_0}{\sqrt{2\pi}(\epsilon + \iota s)}, \qquad -\infty < s < \infty, \tag{4.16}$$

where

$$\bar{f}(s) = \frac{1}{\sqrt{2\pi}} \int_0^\infty f(x)\ e^{isx}\ dx, \tag{4.17a}$$

$$\bar{g}(s) = \frac{1}{\sqrt{2\pi}} \int_{-\infty}^0 g(x)\ e^{isx}\ dx. \tag{4.17b}$$

Based on the behaviour of the solution of the problem, the functions $\bar{f}(s)$ and $\bar{g}(s)$ are exponentially bounded at infinity, and their upper bounds are assumed as

$$|\bar{f}(s)| < M\ e^{l_f x}, \quad as \quad x \to \infty \text{ and}$$

$$|\bar{g}(s)| < N\ e^{l_g x}, \quad as \quad x \to -\infty,$$

where $M > 0$ and $N > 0$ are finite constants. Then the functions $\bar{f}(s)$, $\bar{g}(s)$ are analytic in $\gamma > l_f < 0$ and $\gamma < l_g$ respectively. From this analysis, we can say $l_g \geq 0$. Equations (4.15) and (4.16) together give

$$\bar{f}(s) = K(s)\ \bar{g}(s) - \frac{\sigma_0}{\sqrt{2\pi}(\epsilon + \iota\ s)}, \tag{4.18}$$

where $K(s)$ is the W-H kernel of transform parameter s, given by

$$\frac{C_{44}^{(1)}\ H^{(1)} s\ (-1+\frac{(\eta_1-1)-(\eta_1+1)\ e^{-2sH^{(3)}h_1}}{(\eta_1+1)-(\eta_1-1)\ e^{-2sH^{(3)}h_1}}\ e^{-2sH^{(1)}h})}{(1+\frac{(\eta_1-1)-(\eta_1+1)\ e^{-2sH^{(3)}h_1}}{(\eta_1+1)-(\eta_1-1)\ e^{-2sH^{(3)}h_1}}\ e^{-2sH^{(1)}h})-\eta_3\frac{(-1+\frac{(\eta_1-1)-(\eta_1+1)\ e^{-2sH^{(3)}h_1}}{(\eta_1+1)-(\eta_1-1)\ e^{-2sH^{(3)}h_1}}\ e^{-2sH^{(1)}h})}{(1-\frac{(\eta_2-1)-(\eta_2+1)\ e^{-2sH^{(4)}h_1}}{(\eta_2+1)-(\eta_2-1)\ e^{-2sH^{(4)}h_1}}\ e^{-2sH^{(2)}h})}(1+\frac{(\eta_2-1)-(\eta_2+1)\ e^{-2sH^{(4)}h_1}}{(\eta_2+1)-(\eta_2-1)\ e^{-2sH^{(4)}h_1}}\ e^{-2sH^{(2)}h})} \tag{4.19}$$

4.4.1 W-H method for the solution of the problem

Let us factorise the kernel $K(s)$ into the following form (sub-section 1.7.3) ,

$$K(s) = K_+(s)\ K_-(s), \tag{4.20}$$

where the functions $K_+(s)$ and $K_-(s)$ are free from zeroes and analytic functions for $\gamma > a_1$ $(a_1 < 0)$ and $\gamma < a_2$ $(a_2 > 0)$, respectively. The aim is to arrange $K(s)$ to be

analytic in the strip as $|s| \to \infty$. Hence, equation (4.20), with the help of equation (4.18), becomes

$$\frac{\bar{f}(s)}{K_+(s)} = K_-(s)\ \bar{g}(s) - \frac{\sigma_0}{\sqrt{2\pi}(\epsilon + \iota\ s)\ K_+(s)}. \tag{4.21}$$

Now, decomposing the last term of the equation (4.21) using the Cauchy integral theorem will have

$$\frac{\sigma_0}{\sqrt{2\pi}(\epsilon + \iota\ s)K_+(s)} = L_+(s) + L_-(s), \tag{4.22}$$

where

$$L_+(s) = \frac{\sigma_0}{\sqrt{2\pi}(\epsilon + \iota s)} \left(\frac{1}{K_+(s)} - \frac{1}{K_+(i\epsilon)} \right), \tag{4.23a}$$

$$L_-(s) = \frac{\sigma_0}{\sqrt{2\pi}(\epsilon + \iota\ s)\ K_+(i\ \epsilon)}. \tag{4.23b}$$

Here, + and - denote the analytic properties of respective functions. The functions $L_+(s)$ and $L_-(s)$ are nonzero analytic functions in $\gamma > a_1$ and $\gamma < \epsilon$ $(\epsilon > 0)$, respectively. Rewriting equation (4.21) using equation (4.22), we get

$$\frac{\bar{f}(s)}{K_+(s)} + L_+(s) = K_-(s)\ \bar{g}(s) - L_-(s). \tag{4.24}$$

equation (4.24) uses the fact that the functions $\bar{f}(s)$, $K_+(s)$, $L_+(s)$, $\bar{g}(s)$, $K_-(s)$ and $L_-(s)$ are all analytic functions in the region for $\gamma \geq l_f, \gamma > a_1, \gamma > a_1$, $\gamma \leq l_g, \gamma < a_2$ *and* $\gamma < \epsilon$, respectively. Since the right side of equation (4.24) is analytic in $\gamma \leq 0$, the left side is analytic in $\gamma \geq 0$, and the shared region of analyticity is hence the line $\gamma = 0$ only. Function in equation (4.24) is an entire function which can be successfully stated using the concept of analytic continuation. For significantly large values of s, the functions $\bar{f}(s)$ and $\bar{g}(s)$ will be bounded, and the functions $K_+(s)$ and $K_-(s)$ tend to $s^{1/2}$.The right side of the equation (4.24) tends to $s^{1/2}$ while the left side of the same equation tends to $s^{-1/2}$ for very large values of s

on $\gamma \geq 0$. Based on the Table 1.5, we may conclude that the right-hand term of the equation (4.26) is a constant function as $s \to \infty$. While the left-hand term tends to zero as $s \to \infty$. Therefore, the only entire function $F(s)$ which satisfies the conditions above must be identically zero. Hence,

$$|F(s)| < M_1|s|^{-1/2},$$
$$|F(s)| < M_2|s|^{1/2}, \quad \text{as } |s| \to \infty.$$

So,

$$F(s) = 0. \tag{4.25}$$

Using equations (4.23)-(4.24), with the help of equation (4.25), we get

$$\bar{f}(s) = \frac{\sigma_0}{\sqrt{2\pi}(\epsilon + \iota\ s)} \left(\frac{K_+(s)}{K_+(i\epsilon)} - 1 \right), \tag{4.26a}$$

$$\bar{g}(s) = \frac{\sigma_0}{\sqrt{2\pi}(\epsilon + \iota\ s)\ K_+(i\epsilon)\ K_-(s)}. \tag{4.26b}$$

Taking $\epsilon \to 0$, the above relations become

$$\bar{f}(s) = \frac{\sigma_0}{\sqrt{2\pi}\ (is)} \left(\frac{K_+(s)}{K_+(0)} - 1 \right), \tag{4.27a}$$

and

$$\bar{g}(s) = \frac{\sigma_0}{\sqrt{2\pi}\ (is)\ K_+(0)\ K_-(s)}. \tag{4.27b}$$

The expression of SIF may be determined from the expression of $K(s)$ at small and large values of s. Consequently, the analytic properties of the kernel are of interest,

$$\lim_{s\to\infty} \frac{K(s)}{s} = \beta_1 = -\frac{C_{44}^{(1)} H^{(1)}}{1 + \eta_3}, \tag{4.28}$$

and

$$\lim_{s\to 0} K(s) = \beta_2 = -\frac{C_{44}^{(1)} H^{(1)}}{h(H^{(1)} + \eta_3 H^{(2)}) + h_1(\eta_1 H^{(3)} + \eta_2\ \eta_3\ H^{(4)})}. \tag{4.29}$$

To factorize $K(s) = K_1(s)K_2(s)$ we begin by choosing a $K_2(s)$ that can be factored by inspection where $lim_{|s|\to\infty} K_2(s) \to \infty$ and $lim_{|s|\to 0} K_2(s) \to 0$. Using the conditions that $K_1(s)$ is analytic and free from zeroes in strip $a_1 < c < \gamma < d < a_2,\ c < 0,\ d > 0$ and $K_1(\infty) = 1$, the function can be split by using Cauchy's integral theorem. As a result

$$K_1(s) = K_1^+(s)\ K_1^-(s)$$

where $K_1^{\pm}(\infty) = 1$ and

$$ln(K_1^+(s)) = \frac{1}{2\pi\iota}\int_{-\infty+\iota c}^{\infty+\iota c} \frac{ln(K_1(\xi))}{\xi - s} d\xi$$
$$ln(K_1^-(s)) = \frac{-1}{2\pi\iota}\int_{-\infty+\iota d}^{\infty+\iota d} \frac{ln(K_1(\xi))}{\xi - s} d\xi$$

From equations (4.20), (4.28) and (4.29),

$$K_+(s) = \frac{\sqrt{\beta_1}\ s^{1/2-\iota\eta}\ \Gamma(1/2+\iota\eta)}{\sqrt{\pi/\cosh(\pi\eta)}}, \tag{4.30a}$$

$$K_-(s) = \frac{\sqrt{\beta_1}\ s^{1/2+\iota\eta}\ \Gamma(1/2-\iota\eta)}{\sqrt{\pi/\cosh(\pi\eta)}}. \tag{4.30b}$$

For a large value of s, equation (4.27a) can be rewritten as

$$\lim_{s\to\infty} \bar{f}(s) = \lim_{s\to\infty} \frac{\sigma_0}{\sqrt{2\pi}\ (is)} \left(\frac{K_+(s)}{K_+(0)}\right), \tag{4.31}$$

Thus, we have

$$\bar{f}(s) = s^{-\frac{1}{2}-\iota\eta}\frac{\sigma_0}{\sqrt{2\pi\frac{\pi}{\cosh\pi\eta}}\,i}\sqrt{\frac{\beta_1}{\beta_2}}\,\Gamma(\frac{1}{2}+\iota\eta) \text{ as } \; s\to\infty, \tag{4.32a}$$

Similarly,

$$\bar{g}(s) = s^{-\frac{3}{2}-\iota\eta}\frac{\sigma_0\,\sqrt{\cosh\pi\eta}}{\sqrt{2\pi}\;i\sqrt{\frac{\beta_1\;\beta_2}{\pi}}\;\Gamma(\frac{1}{2}-\iota\eta)} \text{ as } \; s\to\infty, \tag{4.32b}$$

where $\eta = \frac{1}{2\pi}\ln(\eta_3)$. Applying the Inverse Fourier transform in equations (4.32), the expressions of the above functions are found to be

$$f(x) = \frac{-\sigma_0}{\sqrt{2\pi\cosh(\pi\eta)}}\sqrt{\frac{\beta_1}{\beta_2}}\;\frac{1}{x^{\frac{1}{2}-\iota\eta}}\;e^{-\frac{\pi\eta}{2}}, \tag{4.33}$$

$$g(x) = \frac{\sigma_0}{\sqrt{2\pi}\sqrt{\beta_1\beta_2\cosh(\pi\eta)}}\;\left(\frac{(2\eta+1)-\iota(2\eta-1)}{4\eta^2+1}\right)\;\frac{1}{x^{-\frac{1}{2}-\iota\eta}}. \tag{4.34}$$

4.5 Results

The SIF (K_{III}) for considered model is found as

$$\begin{aligned} K_{III} &= \lim_{x\to 0+}\sqrt{2\pi}\;x^{\frac{1}{2}-\iota\eta}\;\tau_{yz}^{(1)}(x,0) \\ &= \frac{-\sigma_0}{\sqrt{\cosh(\pi\eta)}}\sqrt{\frac{\beta_1}{\beta_2}}\;e^{-\frac{\pi\eta}{2}}. \end{aligned} \tag{4.35}$$

The expression of the normalised SIF for the problem becomes

$$NSIF = \frac{1}{\sqrt{h}\sqrt{\cosh(\pi\eta)}}\sqrt{\frac{\beta_1}{\beta_2}}\;e^{-\frac{\pi\eta}{2}}. \tag{4.36}$$

The crack energy is given by

$$W = \int_{-\infty}^{0} \sigma_{yy}^{(1)} \ (\omega^{(1}(x,0) - \omega^{(2)}(x,0)) \ dx. \tag{4.37}$$

Therefore, the Normalised crack energy is given by

$$\frac{W}{\sigma_0^2 h} = \frac{\sqrt{\pi/\cosh(\pi\eta)}}{\pi h\sqrt{2\beta_1\beta_2}} \ \left(\frac{(2\eta+1) - \iota(2\eta-1)}{4\eta^2+1}\right) \int_{-\infty}^{0} x^{\frac{1}{2}+\iota\eta} dx. \tag{4.38}$$

Over the crack, the distance apart of two surfaces is given by

$$\omega^{(1)}(x,0) - \omega^{(2)}(x,0) = \ \frac{\sigma_0}{\pi}\frac{\sqrt{\pi/\cosh(\pi\eta)}}{\sqrt{2\beta_1\beta_2}} \ \left(\frac{(2\eta+1) - \iota(2\eta-1)}{4\eta^2+1}\right) \ x^{\frac{1}{2}+\iota\eta}. \tag{4.39}$$

To evaluate the size of the region in which overlapping occurs, i.e., the crack surfaces first come to rest, we consider $\cos(\eta \ln(x)) = 0$. We can say that at a distance δ before the end of the crack, the contact takes place where $\delta = e^{\pm\frac{\pi}{2\eta}}$. Hence, the maximum size of δ is $e^{-\frac{\pi}{2\eta}}$ if $\eta > 0$ and $e^{\frac{\pi}{2\eta}}$ if $\eta < 0$.

4.5.1 Particular case

If strips (1) and (3) and strips (2) and (4) are identical, then after mathematical calculations, the problem can be easily reduced to a problem of a semi-infinite crack at the interface of two different orthotropic strips of width h. In this case $\eta_1 = \eta_2 = 1$, $\beta_1 = -\frac{C_{44}^{(1)}H^{(1)}}{1+\eta_3}$ and $\beta_2 = -\frac{C_{44}^{(1)}H^{(1)}}{h(H^{(1)}+\eta_3 H^{(2)})}$. Consider the strips' width $h + h_1$ as h, the SIF at the tip of the crack can be calculated as

$$K_{III}^{*} = -\frac{\sigma_0\sqrt{2}}{1+\eta_3}\sqrt{h(H^{(1)} + \eta_3 H^{(2)})} \tag{4.40}$$

4.6 Numerical results and discussion

4.6.1 Validation

The validation process for the current study was conducted to ensure its reliability and accuracy. In the referenced work by K. Somashri et al. [96], the authors investigated the dynamics of a moving crack within a strip that is bonded to a semi-infinite orthotropic medium. In the present research, the parameters were reduced to facilitate a comparative analysis. The results from both the study are illustrated in Figure 4.2, which depicts a detailed graphical representation of the outcomes. Notably, the findings indicate a remarkable correlation across various values at $h = 2.0,\ 4.0,\ 6.0$. This consistency suggests that the results of the current study align closely with those documented in the earlier work, thereby reinforcing the validity of the approach and the robustness of the findings.

This agreement between the two studies not only contributes to the existing body of knowledge on crack mechanics in orthotropic materials but also corroborates the methodologies employed in both investigations. Therefore, it can be confidently asserted that the validation process confirms the accuracy of the results obtained in this study, thereby enhancing their applicability in practical scenarios involving similar material and structural conditions.

4.6.2 Results and discussion

Some analytic results of the semi-infinite moving crack are calculated from equations (4.35)-(4.39) for The antiplane problem. This section provides numerical results to illustrate the analytic results for different parameters' dependencies on NSIF, crack energy and SMF for the considered materials. The elastic properties of the

orthotropic materials used in these calculations are given in Table 4.1. Firstly, the NSIF is plotted for different values of h_1/h and $V/C_s^{(1)}$ for different particular cases, as shown in Figure 4.3, 4.4, 4.5. For this case, strip 1 is taken as Epoxy; strip 2 is Aluminium, strip 3 is Graphite Epoxy and strip 4 is taken as Carbon fibre. Here, the NSIF increases when outer strips 3 and 4 are wider. The dependency of NSIF on crack velocity is shown in Figure 4.3 and 4.5. As the crack velocity increases and approaches shear wave velocity C_s, the NSIF decreases and tends to zero. Next, the NSIF is plotted for different values of h_1/h and $V/C_s^{(1)}$ as shown in Figure 4.6, 4.7, 4.8. In this case, strip 1 and strip 2 are bonded between strip 3, which is taken to be the same as strip 4. Strip 1 is taken as Epoxy, strip 2 is Aluminium, and strips 3 and 4 are Graphite Epoxy. The NSIF, in this case, increases when the width of outer strips 3 and 4 increases, i.e. as the strip width h_1 increases, NSIF increases, as seen in Figure 4.7, 4.8. The dependency of NSIF on crack velocity is shown in 4.6, 4.8. As the crack velocity increases and approaches shear wave velocity $C_s^{(1)}$, the NSIF decreases and tends to zero. Compared with the first case, there is more steepness in the curves in the second case, representing a faster-increasing rate in NSIF when strip 3 is the same as strip 4. This behaviour can be justified because of the change in values of elastic constants of strip 4, which has impacted the values of NSIF.

The NSIF is plotted for different values of h_1/h and $V/C_s^{(1)}$ as shown in Figure 4.9, 4.10, 4.11. In this case, strip 1 and strip 3 are taken as Graphite Epoxy, and strips 2 and 4 are taken as Aluminium. The NSIF, for this case, increases when the width of the outer strips 3 and 4 increase. The dependency of NSIF on crack velocity is shown in Figure 4.9, 4.11. As the crack velocity increases and approaches the shear wave velocity $C_s^{(1)}$, the NSIF decreases and tends to zero. Compared with previous cases, the values of NSIF are slightly higher in this case, but the curves show similar

behaviour.

For the same material choices, the graphs have been plotted to show the dependency of corresponding elastic constant ratios of two materials on NSIF. As shown in Figure 4.12, 4.13, when $C_{44}^{(1)} < C_{44}^{(2)}$, then values of NSIF decreases as $C_{44}^{(1)}$ becomes more smaller as compared to $C_{44}^{(2)}$ but when $C_{44}^{(1)} > C_{44}^{(2)}$, NSIF decreases with increasing values of $C_{44}^{(1)}$. This is because of the shear wave velocity $C_s^{(1)}$ dependency on the elastic constants. The lesser the value of $C_s^{(1)}$, the more will be the value of the SIF.

The absolute energy release of the semi-infinite crack is depicted in Figure 4.14, 4.15, 4.16. Figure 4.14 plots the absolute crack energy vs. crack length for different strips' width ratios. Crack propagation velocity is kept fixed to show the variation in crack energy dependent on h_1/h. As the crack length increases, the energy released increases with increasing values of h_1/h. Figure 4.15 plots the absolute crack energy vs. propagation velocity for fixed strip width ratios. It is seen that the crack energy increases with increasing crack length when V/C_s increases. Figure 4.16 is the 3-D plot for crack energy and its dependency on h_1/h and V/C_s.

In Figure 4.17, we have endeavoured to find the SIF of the considered composite structure over the crack at the interface of the bonded dissimilar materials, as considered in section 5. Here, we aim to show the effect of the exterior strips on the particular case of the considered mathematical model through the stress magnification factor (SMF). From Figure 4.17, SMF increases as the strips' width increases. Figure 4.17 clearly shows the amplification of the nature of the semi-infinite crack due to the presence of exterior strips 3 and 4.

	C_{44} (GPa)	C_{55} (GPa)	ρ (gm/cm^3)
Epoxy	0.176	0.176	1.155
Carbon fiber	6.15	6.15	1.5
Graphite Epoxy	0.361	.565	1.59
Aluminium	2.65	2.65	2.8

TABLE 4.1: Material properties for the considered orthotropic materials.

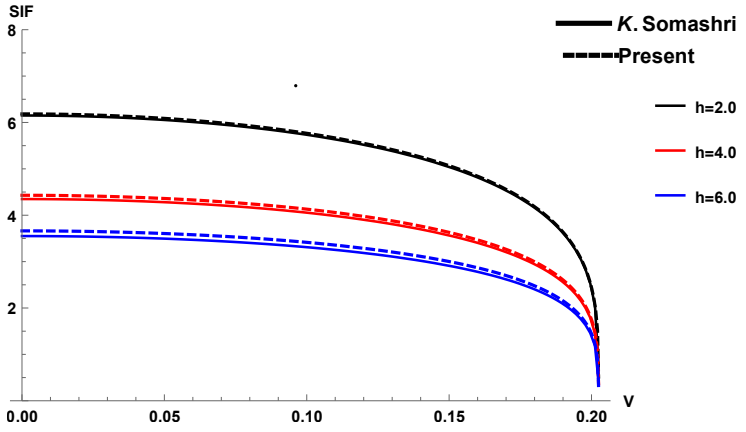

FIGURE 4.2: Plot of stress intensity factor vs. crack velocity for different values of h.

4.7 Conclusion

Through the present scientific contribution, the authors have achieved five goals. The first one is the appropriate use of the W-H method to handle the W-H and the W-H dual equations by splitting those into two parts using a contour in the complex plane. The second one is the finding of the asymptotic expression of the SIF at the tip of the semi-infinite crack situated at the interface of two dissimilar orthotropic media. In most of the interfacial semi-infinite crack problems, the researchers have found the SIF considering $\lim_{x\to 0^+} \sqrt{2\pi x}\ \sigma_{yy}^{(1)}(x,0)$, which means assuming the order of the singularity of the crack lying at the interface is $r^{-1/2}$ which is fundamentally wrong as it is true for embedded crack. For the interface, it will be $r^{-1/2+\iota\nu}$, ν is real.

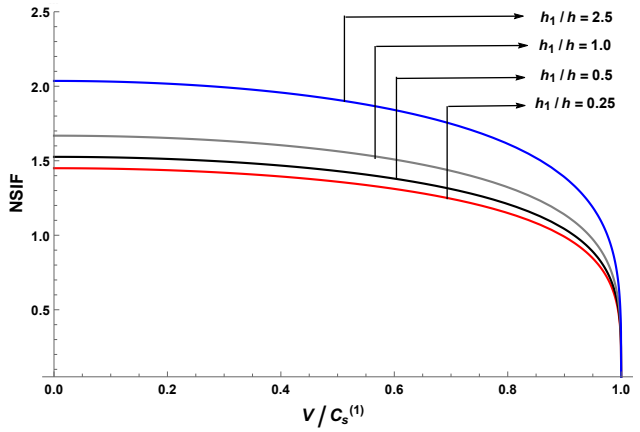

FIGURE 4.3: Plot of normalised stress intensity factor vs. crack velocity for different h_1/h ratios for the considered model with dissimilar strips.

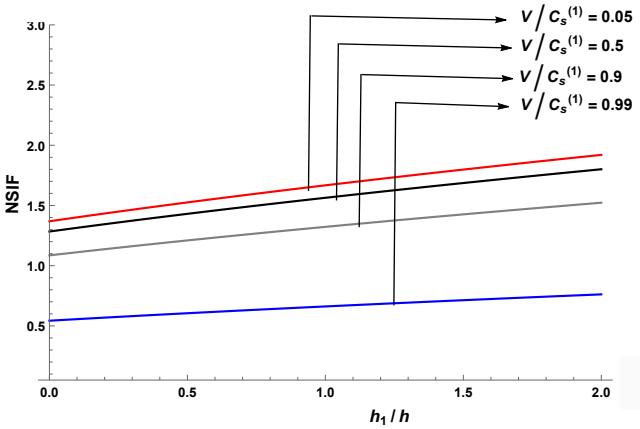

FIGURE 4.4: Plot of normalised stress intensity factor vs. strip width ratios for different crack velocities for the considered model with dissimilar strips.

Therefore, we have found SIF using $\lim_{x\to 0^+} \sqrt{2\pi}\ x^{-1/2+\iota\eta}, \eta = \frac{1}{2\pi}\ln(\eta_3)$. Therefore, the effort to find SIF is mathematically correct, and it will give a new direction to the researchers working in the area of research in question. The third one is finding the analytical expression of the normalised crack energy and then showcasing the pictorial presentations of the absolute crack energy for different crack velocities and depths of the composite. The fourth one is finding the exact length of the meeting of

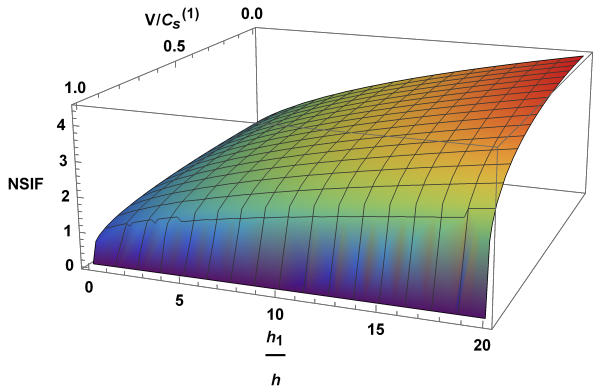

FIGURE 4.5: Plot of normalised stress intensity factor vs. crack velocity vs. h_1/h ratios for the considered model with dissimilar strips.

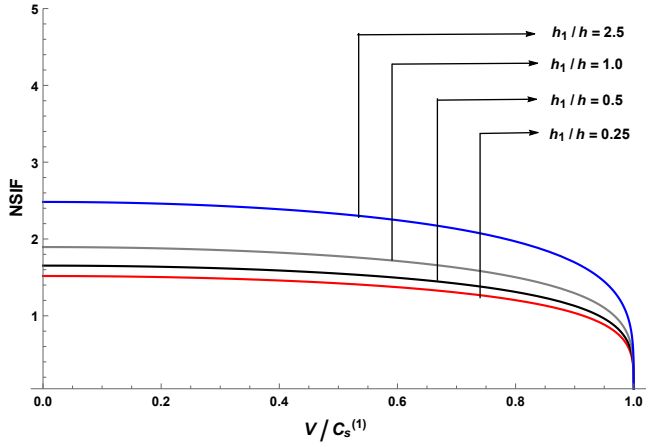

FIGURE 4.6: Plot of normalised stress intensity factor vs. crack velocity for different h_1/h ratios for the considered model with two dissimilar strips sandwiched between similar strips.

the two faces of the crack before its tip. This contribution is also the first of its kind for interfacial semi-infinite crack. The last one is the drive for showing graphically the effects of the exterior strips on the bonded strips containing the semi-infinite crack situated at their interfaces through SMF for various depths of the strips of the composite material and various crack velocities for different particular cases.

The problem has been extended to conducting a crack model where, in real-life scenarios, the cracks need not be empty and insulated; there might be some medium,

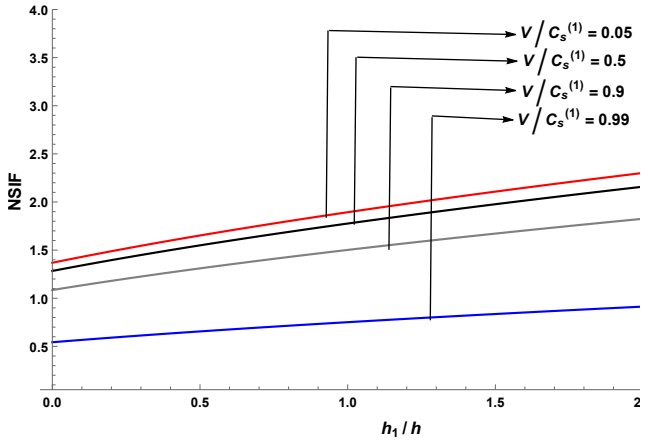

FIGURE 4.7: Plot of normalised stress intensity factor vs. strip width ratios for different crack velocities for the considered model with two dissimilar strips sandwiched between similar strips.

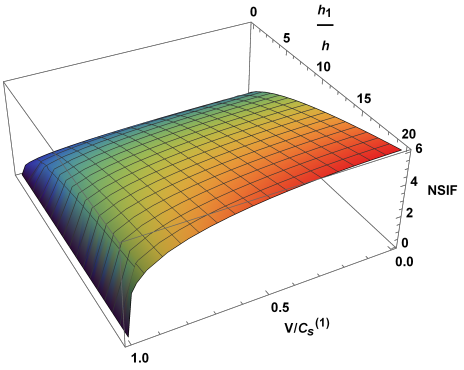

FIGURE 4.8: Plot of normalised stress intensity factor vs. crack velocity vs. h_1/h ratios for the considered model with two dissimilar strips sandwiched between similar strips.

viz. air, water, etc., trapped inside the cracks, which have their thermal conductivity.

The next chapter addresses the partially insulated crack problem.

****

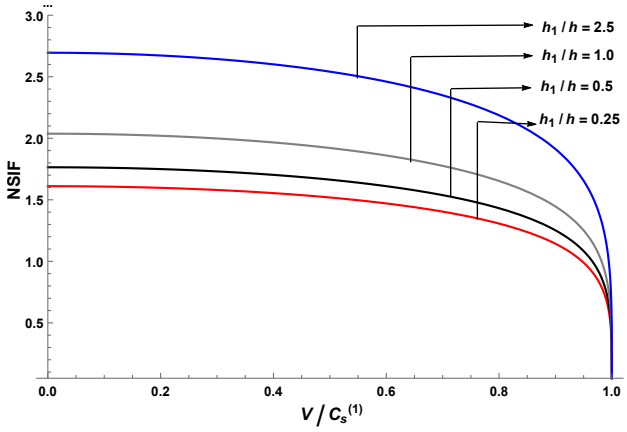

FIGURE 4.9: Plot of normalised stress intensity factor vs. crack velocity for different h_1/h ratios when strip 3 is the same as strip 1 and strip 4 is the same as strip 2.

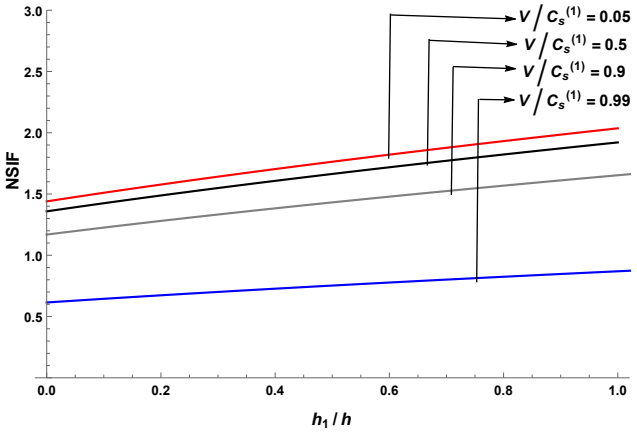

FIGURE 4.10: Plot of normalised stress intensity factor vs. strip width ratios for different crack velocities when strip 3 is the same as strip 1 and strip 4 is the same as strip 2.

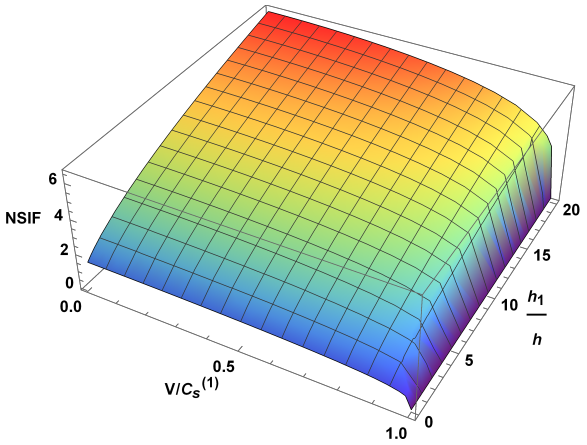

FIGURE 4.11: Plot of normalised stress intensity factor vs. crack velocity vs. h_1/h ratios when strip 3 is the same as strip 1 and strip 4 is the same as strip 2.

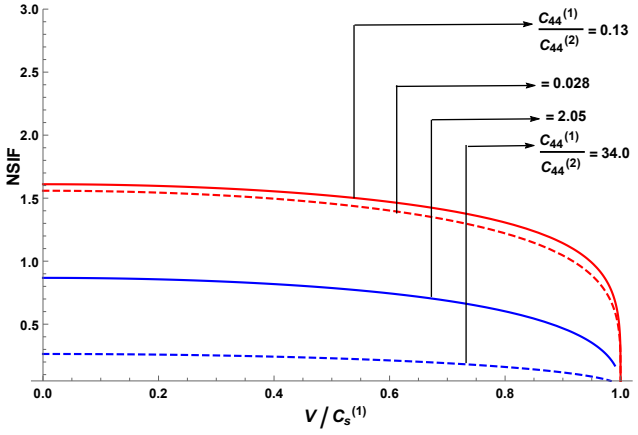

FIGURE 4.12: Plot of normalised stress intensity factor vs. crack velocity for different C_{44} ratios for two bonded strips.

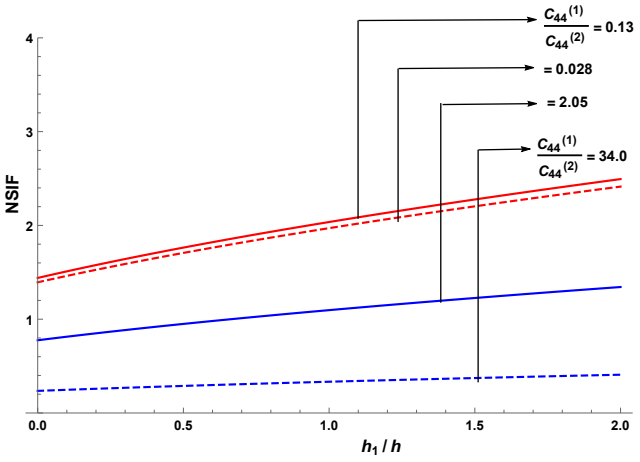

FIGURE 4.13: Plot of normalised stress intensity factor vs. h_1/h for different C_{44} ratios for two bonded strips.

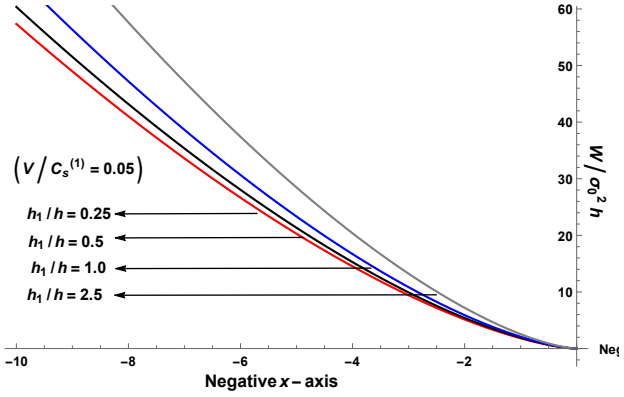

FIGURE 4.14: Plots of absolute crack energy for different h_1/h and $V/C_s^{(1)}$ (a)Abs$(W/\sigma_0^2 h)$ vs. crack length for various h_1/h.

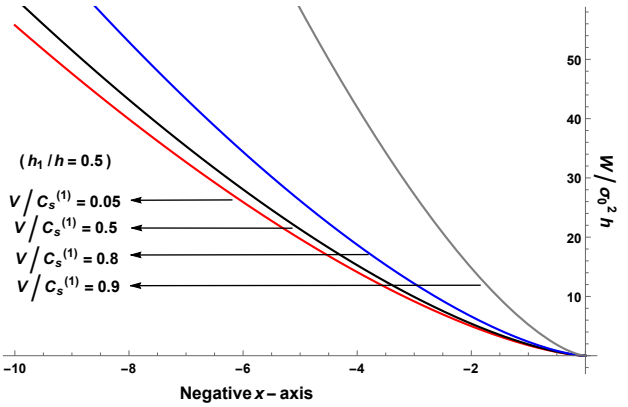

FIGURE 4.15: Plots of absolute crack energy for different h_1/h and $V/C_s^{(1)}$ Abs$(W/\sigma_0^2 h)$ vs. crack length for various $V/C_s^{(1)}$.

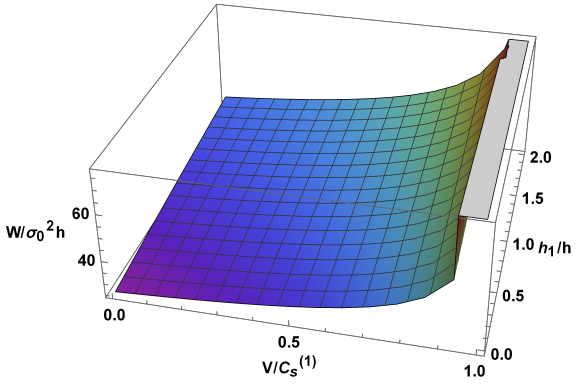

FIGURE 4.16: Plots of absolute crack energy for different h_1/h and $V/C_s^{(1)}$.

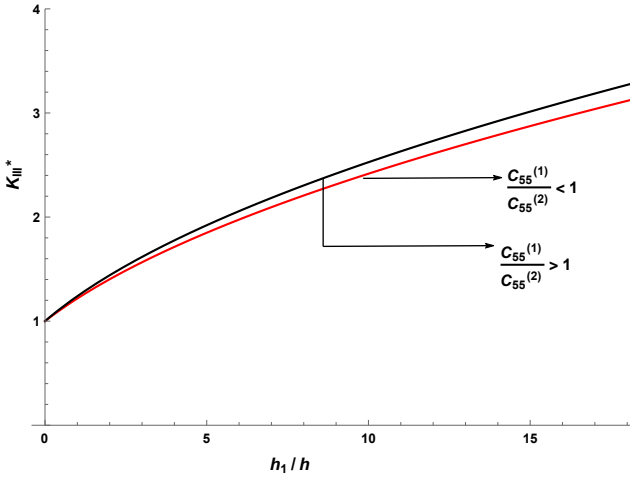

FIGURE 4.17: Plots of the effects of $C_{55}^{(1)}/C_{55}^{(2)}$ on the stress magnification factor for the considered model.